█ **Prussian Blue Analogues** | *Reviews Showcase* |

# How to Build Prussian Blue Based Water Oxidation Catalytic Assemblies: Common Trends and Strategies

T. Gamze Ulusoy Ghobadi,[b] Ekmel Ozbay,[c] and Ferdi Karadas*[a, b]

Abstract: Prussian blue (PB) and its analogues (PBAs) have at least a three-century-long history in coordination chemistry. Recently, cobalt-based PBAs have been acknowledged as efficient and robust water oxidation catalysts. Given the flexibility in their synthesis, the structure and morphology of cobalt-based PBAs have been modified for enhanced catalytic activity under electrochemical (EC), photocatalytic (PC), and photoelectrochemical (PEC) conditions. Here, in this review, the work on cobalt-based PBAs is presented in four sections: i) electrocatalytic water oxidation with bare PBAs, ii) photocatalytic processes in the presence of a photosensitizer (PS), iii) photoelectrochemical water oxidation by coupling PBAs to proper semiconductors (SCs), and iv) the utilization of PBA-PS assemblies coated on SCs for the dye-sensitized photoelectrochemical water oxidation. This review will guide readers through the structure and catalytic activity relationship in cobalt-based PBAs by describing the role of each structural component. Furthermore, this review aims to provide insight into common strategies to enhance the catalytic activity of PBAs.

1. Introduction

Cyanide rapidly reacts with metal ions, labeling itself a toxic and dangerous molecule. Despite its bad reputation, it can be used to connect proper functional units to prepare low-cost and non-toxic multifunctional materials on a large scale.[1–6] The most well-known family of cyanide-based compounds is Prussian blue (PB) and its analogues (PBAs), which can be facilely synthesized by mixing a hexacyanometalate complex with a 3d transition metal ion to afford mixed-metal cyanometalates. These materials, with a history dating back to the beginning of the 18th Century, are known as microporous coordination polymers with a three-dimensional open framework structure. In a PB structure, metal cations are connected through cyanide bridging ligands, forming a cubic coordination network with the general molecular formula $A_nM_x[M'(CN)_6]\cdot nH_2O$ (A = alkali-metal ions, M and M' = transition metal ions). Figure 1 shows the typical crystalline structure of a cobalt-based PBA, CoFe PBA, in which M = Co, M' = Fe. Given the diversity (adjustable metal active sites), high porosity, fast electron transfer, earth-abundance, and simple synthesis of PBAs, they have been investigated as promising materials in a wide range of applications including magnetism,[7] photomagnetism,[8] alkaline-ion batteries,[9–11] gas capture and storage,[12,13]
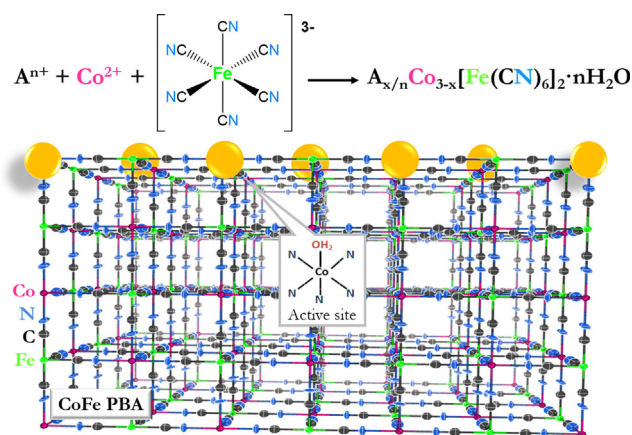
Figure 1. Synthesis and general structure of $A_nCo_x[Fe'(CN)_6]\cdot nH_2O$ (A = H+, Li+, Na+, K+, Rb+, Cs+, Mg2+, Ca2+). Here, nitrogen-coordinated Co sites and carbon-coordinated Fe ones are bridged by cyanide (CN) groups to form an open framework. Catalytically active cobalt sites, which are surrounded by at least one water molecule, are highlighted with orange spheres. Alkali metal ions residing in the tetrahedral positions of the cubic structure are omitted for clarity.

[a] Prof. F. Karadas
Department of Chemistry
Bilkent University
Ankara 06800 (Turkey)
E-mail: karadas@fen.bilkent.edu.tr

[b] T. G. Ulusoy Ghobadi, Prof. F. Karadas
Institute of Materials Science and Nanotechnology
UNAM—National Nanotechnology Research Center
Bilkent University
Ankara 06800 (Turkey)

[c] Prof. E. Ozbay
NANOTAM—Nanotechnology Research Center
Department of Electrical and Electronics Engineering
Department of Physics
Bilkent University
Ankara 06800 (Turkey)

The ORCID identification number(s) for the author(s) of this article can be found under:
https://doi.org/10.1002/chem.202004091.

Selected by the Editorial Office for our Showcase of outstanding Review-type articles (www.chemeurj.org/showcase).

sensors,[14] H_2O_2 reduction,[15] electrochromic devices,[16,17] and biomedicine.[2,18] PBAs have recently received attention as potential robust and efficient water oxidation catalysts (WOCs) for efficient and scalable water splitting devices. Since the benchmark study in 2013 by Galán-Mascarós and co-workers,[19] PBAs have been found to operate efficiently under electrocatalytic (EC), photocatalytic (PC), and photoelectrochemical (PEC) conditions. Detailed discussions on various water splitting platforms were presented in our earlier review.[20,21] In addition, several reviews have recently focused on PB derived multimetallic oxides, sulfides, and phosphides rather than cyanide-based coordination networks themselves.[22–26] This review, however, provides a comprehensive overview of cyanide-based water oxidation catalytic assemblies to exploit the role of each structural unit in a PB structure to the water oxidation process.

2. Water Oxidation

The use of catalysts in water oxidation has gained new momentum after the seminal work on the water oxidation catalytic activity of cobalt oxides in the presence of a phosphate

Chemistry–A European Journal

Minireview
doi.org/10.1002/chem.202004091

**Chemistry
Europe**
European Chemical
Societies Publishing

buffer (Co-Pi).[27,28] This work has also accelerated the studies on heterogeneous catalysis with bulk systems. In 2013, a cobalt-based PBA also came into play as one of the first non-oxide heterogeneous WOCs.[19] The impact of this work is two-fold: 1) it provides new insight into the water oxidation mechanism by demonstrating that an oxo-bridge is not essential for water oxidation catalysis; 2) a new family of heterogeneous catalysts is introduced to the field.

Cobalt hexacyanoferrates can be regarded as non-stoichiometric coordination network compounds, in which the Co/Fe atomic ratio can vary between 1 to 2, depending on the synthesis, counter alkali metal cation, and the oxidation state of iron. The network consists of catalytically inactive iron sites surrounded by six cyanide groups, which serve as a bridging group between cobalt sites. A cobalt ion, on the other hand, is surrounded with a combination of nitrogen atoms of cyanide groups and water molecules forming a coordination sphere with a general formula, $Co^{II}(NC)_x(OH_2)_{6-x}$. The cobalt site in a PB structure can easily be oxidized to its higher oxidation states, which makes it an ideal catalytic site for water oxidation. All the PB-based WOCs studied to date are, therefore, cobalt-based ones. Several key features that make cobalt-based PBAs ideal catalytic assemblies for water oxidation are listed below and are shown in Figure 2.
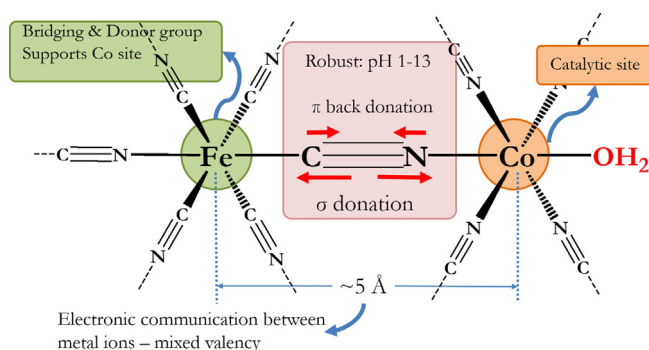
Figure 2. Characteristic features of each constituent in a CoFe PBA.

Simple synthesis: Given the reactivity of both the carbon and nitrogen atoms of the cyanide group, a cyanide-based coordination polymer could be obtained by just mixing a cyanometalate complex with a transition metal ion resulting in a color change and a precipitate. The purification of the powder is generally performed by using aqueous or alcoholic solvents at room temperature under air with a high yield.

Diverse morphology: The flexible synthesis of PBAs can be modified to achieve a morphology that suits the needs of the desired application. Capping ligands and surfactants can easily be incorporated into the synthesis to control the surface chemistry, morphology, crystallinity, and the particle size of PBAs.[29–31]

Diversity: Given the straightforward synthesis, desired alkali (H, Li, Na, K, Rb, Cs), alkaline earth (Mg, Ca), and 3d transition metal ions (Cr, Mn, Fe, Co, Ni, Cu, Zn) can be incorporated into the PB structure, which enables systematic investigation of the role of each component in a specific application.[32–34]

Earth abundance: As all of the components in PBAs are earth abundant, non-toxic, and low-cost precursors, they can be utilized for building scalable and low-cost electrochemical devices and water splitting cells.

Robustness: Unlike most of the common oxide-based WOCs, PBAs exhibit exceptional stabilities even under harsh acidic conditions.[35] They can efficiently operate at almost all pH values (pH 1–13), which is highly desirable for water splitting devices. For example, a FeFe PB is an FDA approved drug for radiocesium, which is taken orally as it is stable even against gastric acid, pH 1.5.[36–39] The superior stability of PBAs under both neutral and acidic conditions could be attributed to strong σ-donation (mainly owing the negative charge of the

Turkan Gamze Ulusoy Ghobadi received her B.S. degree in Chemical Engineering from Ankara University, Turkey, in 2012. She subsequently joined the National Nanotechnology Research Center (UNAM), Institute of Materials Science and Nanotechnology, Bilkent University, Turkey, and obtained her M.Sc. degree in 2015. Currently, she is pursuing her Ph.D. degree in the same department under the joint supervision of Asst. Prof. Ferdi Karadas and Prof. Ekmel Ozbay. Her current research interests involve the design, synthesis, and characterization of (photo)electrochemical materials for energy conversion devices.

Prof. Dr. Ekmel Ozbay received M.S. and Ph.D. degrees from Stanford University in electrical engineering, in 1989 and 1992. He worked as a postdoctoral research associate at Stanford University and he worked as a scientist in Iowa State University. He joined Bilkent University (Ankara, Turkey) in 1995, where he is currently a full professor in the Physics Department and EEE Department. In 2003, he founded the Bilkent University Nanotechnology Research Center (NANOTAM) where he leads a research group working on nanophotonics, nanometamaterials, nanoelectronics, GaN/AlGaN MOCVD growth, and GaN-based devices. He is the 1997 recipient of the Adolph Lomb Medal of OSA and 2005 European Union Descartes Science award. He has worked as an editor for Nature Scientific Reports, Optics Letters, PNFA, and IEEE JQE journals. He has published 420+ articles in SCI journals. His papers have received 25 000+ SCI citations with an SCI h-index of 79. He has given 145+ invited talks at international conferences. He recently became the CEO of a spin-off company: AB-MicroNano Inc.

Asst. Prof. Ferdi Karadas received his Ph.D. in molecular magnetism and inorganic coordination compounds in 2009 from Texas A&M University in Texas, USA, under the supervision of Prof. Kim R. Dunbar. Since 2013, he has been a professor in the Department of Chemistry, Bilkent University, Turkey. His research is focused on the development of new materials and molecular hybrid systems for water oxidation and reduction, electrocatalysis, and dye-sensitized photoelectrocatalytic systems.

Chemistry–A European Journal

Minireview
doi.org/10.1002/chem.202004091

Chemistry Europe
European Chemical
Societies Publishing

ligand) and π-back donation (owing to the empty relatively low-energy π* orbitals) between the metal ion and cyanide group, which yields a much lower solubility constant compared with metal oxides (K_{sp} for PB is 10^{-41} whereas it is approximately 10^{-15} for cobalt oxides). The superior pH endurance, therefore, makes PBAs strong candidates as robust WOCs. It is noteworthy that catalytic studies with PBAs above pH 13 should be performed with caution as they transform to metal hydroxides, which could also exhibit efficient water oxidation catalytic activities.

Porosity: PBAs are considered as one of the oldest coordination polymers and they exhibit a microporous nature as the cyanide bridging group creates microchannels with a size of approximately 5 Å, which enables the access of small molecules including water and oxygen, see Figure 2. Moreover, all PBAs exist in the same cubic structure regardless of the metal ions used and the metal-to-metal stoichiometric ratio. For example, the cobalt-to-iron ratio is generally greater than one to provide a charge balance.[40] Small voids occur in the structure owing to the partial absence of cyanoferrate groups. Therefore, cobalt sites coordinated to at least one water molecule are present even in the subsurface of the structure. The catalytic activity of these interior defect sites is confirmed with a recent study, which suggests that a PB layer of around 7 nm thickness participates actively in the catalytic water oxidation process.[41]

Fast electron transfer: Short cyanide linker (M-CN-M′ distance is ≈5 Å) provides fast electronic communication between metal ions. Heteronuclear metal cyanide compounds generally fall into Class II based on Robin–Day classification revealing the partial localization of distinct valences.[42–46] Both metal sites in a CoFe PBA exhibit easily accessible $M^{2+/3+}$ redox processes. Whereas $Co^{2+} \rightarrow Co^{3+}$ oxidation is one of the critical steps in a water oxidation process, the $Fe^{2+/3+}$ redox process is utilized to increase the electron density of electron-deficient catalytic cobalt sites for enhanced water oxidation activity. Therefore, iron sites serve as bridging and donor groups in CoFe PBAs. The electronic effect of iron sites will be discussed in more detail in Section 2.4. This unique behavior could be utilized to provide a fast electron transfer between metal ions to mediate the charge transfer during the water oxidation process.

2.1 Electrocatalytic (EC) water oxidation

Electrocatalytic water splitting is mainly limited by the high overpotentials of both the hydrogen evolution and oxygen evolution reactions. The complex multistep proton-coupled electron transfer ($4e^-$ process), water oxidation, is particularly considered as the most challenging half-reaction of the water splitting process. Here, CoFe PBAs advance as active electrocatalysts to accelerate the sluggish oxygen evolution reaction kinetics by reducing the activation energy of the reaction. Catalytic studies performed on a series of metal hexacyanoferrates (M = Mn, Fe, Co, and Ni) indicate that cobalt is the most active catalytic site in PB structures.[47] In a classic three-electrode setup (Figure 3 a), a typical CoFe PBA modified electrode, regardless of the synthetic method, exhibits two characteristic features in the anodic region: i) a quasi-reversible band at around 0.9 V (vs. Ag/AgCl electrode) at pH 7, which is attributed to a $Co^{2+/3+}$ redox process just before and ii) an irreversible peak owing to the catalytic water oxidation process.[19,48] The electrode is extremely stable under neutral conditions as confirmed by long-term chronoamperometry and chronopotentiometry experiments.[35] The cobalt sites in a PB framework are estimated to be more active than those in a bulk Co_3O_4 structure. Electrochemical studies reveal that a turnover frequency (TOF) of 2.6×10^{-3} s^{-1} could be obtained at an overpotential (η) of 410 mV for Co_3O_4 whereas it is only 305 mV for a CoFe PBA modified electrode.[19] The cyanide linker, however, results in a lower surface concentration on the order of 'nmol cm^{-2}' compared with bulk oxides (on the order of 'µmol cm^{-2}'), as the distance between the neighboring cobalt sites in a PB structure is approximately 10 Å (it is approx. 3–4 Å for oxides and sulfides). The majority of the earlier research conducted on electrocatalytic water oxidation with PBAs, therefore, revolved around increasing the surface concentration of active catalytic sites by either varying the cobalt precursor, changing the cyanide precursor, using support materials, or a combination of these. These strategies are highlighted below with practical experimental methods:

i) Changing the cyanide precursor: The inspection of the effect of a structural parameter on the catalytic activity in bulk PBA systems can be quite challenging, as a slight change in
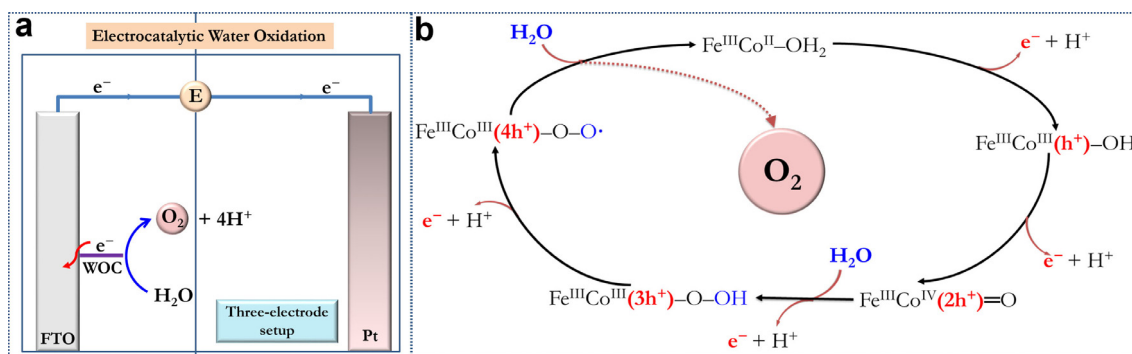
Figure 3. Schematic of (a) a general EC water oxidation setup including a WOC deposited on FTO-coated glass, reference electrode (not shown), and a metal cathode that is immersed in an electrolyte and connected by an external electric wire, and (b) the responsible proton-coupled electron transfer (PCET) mechanism for EC water oxidation with CoFe PBAs.

the synthetic conditions or the precursors generally varies the morphological and electronic properties of the assembly. In the electrocatalytic water oxidation studies of CoFe PBAs, morphological changes have been monitored with the surface concentration of catalytic cobalt sites whereas electronic properties of the catalytic sites are compared based on the TOF value. In 2013, Galán-Mascarós and co-workers employed a well-established potentiostat deposition method to prepare a CoFe PBA-modified FTO-coated glass with a surface concentration of approximately 1.4 nmol cm^{-2}.[19] A similar value is obtained when a CoFe PBA-modified electrode is prepared with a drop-casting method.[49] In addition to a long distance between cobalt sites, the origin of the relatively low surface concentration in CoFe PBAs is also due to their high crystallinities as depicted by sharp diffraction peaks in their powder XRD patterns. Our group recently found that an amorphous CoFe coordination polymer could be obtained when the symmetric hexacyanoferrate complex is replaced with a polymer-bound pentacyanoferrate precursor.[48] The polymer herein serves as a capping group, which limits the dimensionality of the cyanide-based network structure. The change of the morphology from a crystalline structure to an amorphous one leads to a seven-fold increase in the surface concentration. In other words, the amorphization of the reactive surface or decreasing the degree of crystallinity of the catalytic structure allows for better participation of the catalytic site to the water oxidation process and its easy transformation to the required intermediates.[50] Later, Bonacin and co-workers employed the [Fe(CN)$_5$(isn)] complex (isn = isonicotinate) to prepare a CoFe PBA with a surface concentration of around 6.0 nmol cm^{-2}.[51] Varying the number of cyanide groups coordinated to the cyanometalate group, therefore, provides a good opportunity to enhance the number of catalytic sites and/or defects on the surface for an oxygen evolution reaction.

A list of electrocatalytic water oxidation activities with important electrocatalytic parameters, including overpotentials, Tafel slopes, and TOF of PBAs, is provided in Table 1.

Coordinatively saturated iron ions are considered to be innocent sites in the catalytic process. In CoFe PBAs, the electron density on one metal site, however, affects the other one as PBAs fall in Class II mixed-metal compounds based on Robin–Day classification.[42–46] Electrochemical studies performed on CoFe PBAs indicate that the Fe$^{2+/3+}$ and Co$^{2+/3+}$ redox potentials are close to each other, which makes them difficult to differentiate from each other.[40] A series of cobalt hexacyanometalates, Co$_x$[M(CN)$_6$], M = Fe$^{2+/3+}$, Co^{3+}, and Cr^{3+}, was studied to elucidate the effect of the hexacyanometalate group on the water oxidation activity of cobalt sites.[49] Although the morphology and surface concentration are similar, the TOF value of the cobalt site in CoM PBAs ranges dramatically from 3× 10^{-3} s^{-1} for Co^{II}Co^{III} PBA to 5×10^{-2} s^{-1} for Co^{II}Fe^{II} PBA. Therefore, the hexacyanometal group bears a clear *electronic effect* on the catalytic activity of cobalt sites. A catalytic mechanism is also proposed, which is supported by experimental studies and theoretical calculations (Figure 3b). The 4e$^-$ mechanism, similar to the oxide-based mechanism, involves the oxidation and activation of the catalytic site by four proton-coupled electron transfer (PCET) to yield a high-valent metal-oxo species. This active species is attacked by a nucleophilic water molecule to form a peroxo species, which is then released as an oxygen molecule. As the relatively long distance between two cobalt sites in a PB structure prevents the collaboration of active sites for catalysis, the 4e$^-$ water oxidation process is considered to occur on just one cobalt site. Similar to the water oxidation mechanism in cobalt oxides, one of the two critical steps, the oxidation of Co^{3+} to a higher oxidation state or the nucleophilic attack of the water molecule to a cobalt-oxo species, should be the rate-determining step in PB systems. The nature of these two steps differs from each other as an increase in the

Table 1. A comparison of the electrocatalytic water oxidation activities of PBAs reported in the literature.

Catalyst[a]	Formula	η_{onset} [mV]	η_{1mA}[b] [mV]	pH	TOF [s^{-1}]	Tafel slope [mV dec^{-1}]	Prep method	Ref
[Co-Fe]	K$_{2x}$Co$_{(2-x)}$[Fe(CN)$_6$] (0.85 < x < 0.95)	N/A	>600	7	2.6×10^{-3} at η=305 mV 2×10^{-3} at η=300 mV 0.5 at η=550 mV	85–95	Electrodeposition	[19]
[Co-Fe(CN)$_5$-P4VP]	Co$_{1.5}$[Fe(CN)$_5$P4VP]	360	510	7	2.6×10^{-3} at η=284 mV	111	Precipitation+Spin-coating	[48]
[Co-Fe][c]	Co$_{1.5}$[Fe(CN)$_6$]	N/A	500	7	N/A	91	Chemical etching of Co(OH)(CO$_3$)$_{0.5}$	[35]
[Co-Co^{III}]	K$_{0.38}$Co$_{1.31}$[Co(CN)$_6$]	283	565	7	5×10^{-2} at η=400 mV	99	Precipitation+drop-cast	[49]
[Co-Cr^{III}]	K$_{0.41}$Co$_{1.29}$[Cr^{III}(CN)$_6$]	303	598	7	5×10^{-3} at η=400 mV	96	Precipitation+drop-cast	[49]
[Co-Fe^{III}]	K$_{0.31}$Co$_{1.35}$[Fe^{III}(CN)$_6$]	323	717	7	4.4×10^{-3} at η=400 mV	127	Precipitation+drop-cast	[49]
[Co-Fe^{II}]	K$_{0.70}$Co$_{1.65}$[Fe^{II}(CN)$_6$]	343	1079	7	3×10^{-3} at η=400 mV	121	Precipitation+drop-cast	[49]
[Co-Fe]/Sb-SnO$_2$	Co$_{1.5}$[Fe(CN)$_6$]	520	N/A	7	N/A		Precipitation+spraying	[52]
[Co$_{0.9}$Fe$_{0.1}$-Co]	Co$_{1.34}$Fe$_{0.15}$[Co(CN)]$_6$	303	569	7	2.6×10^{-3} at η=295 mV	104	Precipitation+drop-cast	[53]
[Co$_{0.5}$Fe$_{0.5}$-Co]	Co$_{0.75}$Fe$_{0.75}$[Co(CN)]$_6$	323	591	7	2.6×10^{-3} at η=312 mV	104	Precipitation+drop-cast	[53]
[Fe-Co]	Fe$_{1.5}$[Co(CN)]$_6$	475	730	7	N/A	112	Precipitation+drop-cast	[53]
[CoFe-isn]	Co$_2$[Fe(CN)$_5$isn]	324	N/A	7	7.0×10^{-3} at η=400 mV	146	Potentiostatic/cyclic deposition	[51]

[a] In a given abbreviation, the metal ions coordinated to the nitrogen end of the cyanide group are given before the dash, and the ones after the dash symbol represent the cyanometalate precursors. For pentacyanometal-based PBAs, the ligand connected to the iron site is given after metal sites. In all PBAs, the oxidation state of the Co^{II} ion is the precursor. [b] η_{1mA} represents the overpotential (mV) at 1 mA cm^{-2}. [c] Overpotential (mV) at 10 mA cm^{-2} is 760 mV.

Chemistry–A European Journal

Minireview
doi.org/10.1002/chem.202004091

Chemistry Europe
European Chemical
Societies Publishing

electron density of catalytic cobalt sites decreases the rate of the former process and increases the latter one. The cyanide stretching frequency (ν_{CN}) is monitored by infrared spectroscopy to evaluate the electron density of cobalt sites as ν_{CN} provides a rough comparison of the electron densities of PBAs. The shift in the cyanide stretch to higher frequencies is well correlated with the enhancement in water oxidation activity in a series of CoM PBAs, which suggests that the nucleophilic attack of the water molecule should be the rate-determining step.

ii) Changing the cobalt precursor: Not only the cyanide precursor but also the nature and coordination environment of cobalt ions play a critical role in the catalytic performance of PBAs. As cyanometalates react rapidly with bare cobalt ions, the growth of the PB structure can be controlled by employing a cobalt precursor with a relatively low solubility product in aqueous solutions. For this purpose, a $Co(OH)_x$-coated FTO electrode was reacted with a hexacyanoferrate solution to afford CoFe PB cubic structures in the 50 nm to 1 μm range by Galán-Mascarós et al.[35] A surface concentration of above 100 nmol cm^{-2} is obtained with these electrodes whereas it is only around 2 nmol cm^{-2} for the previously reported CoFe PBA prepared with an electrodeposition method.[19] This method also allows strong interfacial matching with the FTO surface and PB structures, which leads to a significant enhancement in the electrocatalytic activity (Table 1). Electrocatalytic water oxidation studies were also performed on PBAs with the formula $Co_{3-x}Fe_x[Fe(CN)_6]_2$ to elucidate the role of iron doping in two different studies.[53,54] Although the partial substitution of cobalt sites with iron doping has no significant effect at relatively low current densities, an enhancement at high current densities (above 40 mA cm^{-2}) was obtained mainly owing to faster charge transfer kinetics.
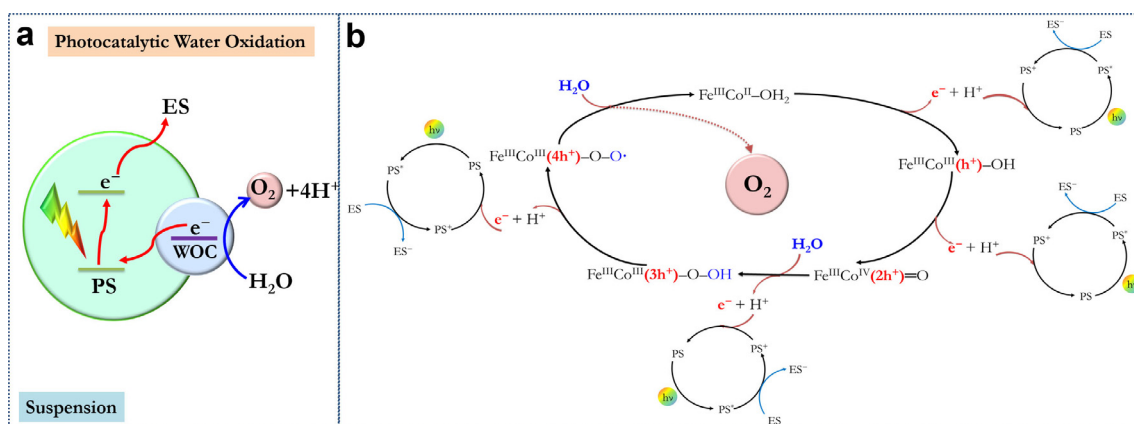
2.2 Photocatalytic (PC) water oxidation

An ideal WOC should not only be efficient and robust but also have matching energy level alignment with a visible-light absorbing component such as a photosensitizer (PS) or a semiconductor (SC). The HOMO level of a CoFe PB structure is generally placed at a slightly lower energy level than the water oxidation half potential, which makes it an ideal catalyst for prospective water splitting cells.

A PS should have a lower HOMO level than that of CoFe PBA for the efficient charge transfer between the PS and the WOC. Once this is achieved, the hole created in the HOMO level of the PS upon excitation can be transferred to the HOMO level of PB to activate the catalytic site (Figure 4a). An electron scavenger (ES) in the electrolyte is necessary to consume the electrons in the LUMO level of the PS, which provides its charge balance by accepting electrons from the water oxidation process (Figure 4b).

One of the well-known photosensitizer–electron scavenger (PS/ES) couples, $[Ru(bpy)_3]^{2+}/S_2O_8^{2-}$, has been commonly used in several studies to evaluate the photocatalytic performance of PBAs.[47] The activities are generally reported through a TOF value or a quantum yield (Table 2). It should be noted that, in earlier studies, FeFe PBAs have also been observed to be active under similar conditions, but with relatively lower activities.[55,56] Recent studies have focused on understanding the photocatalytic process in CoFe PBAs and tuning the activity by changing the constituents of the cyanide network. For example, the substitution of the $[Fe(CN)_6]^{3-}$ component with $[Co(CN)_6]^{3-}$ or $[Pt(CN)_6]^{2-}$ groups enhances the catalytic activity of cobalt sites mainly owing to the above-mentioned electronic effect through a short cyanide bridging group.[57,58] Furthermore, the partial substitution of the hexacyanometal group with a tetracyanometalate one such as the $[Pt(CN)_4]^{2-}$ complex also increases the number of active cobalt sites, which is also reflected in the quantum yield (50%). Unlike electrocatalytic studies, a significant increase in the photocatalytic activity was observed with the partial substitution of cobalt sites with iron. $(Fe_{0.75}Co_{0.25})_3[Co(CN)_6]_2$ was observed to be around 50% more active than $Co_3[Co(CN)_6]_2$, which is attributed to the stabilizing effect of iron sites on the higher oxidation states of active catalytic sites.[58] The role of counter cation, which is largely ignored in most studies, has been investigated by Fukuzumi and co-workers.[59] Interestingly, they observed a remarkable in-

Figure 4. Schematic of (a) a general PC water oxidation setup including a PS, WOC, and ES in an electrolyte, and (b) the responsible PCET mechanism for PC water oxidation with CoFe PBAs.

Table 2. Recent PB-based photocatalysts and their PC performances for the water oxidation process.

Photocatalyst	Formula	TOF [s^{-1}]	Quantum yield	O$_2$ evolved [µmol mg^{-1} h^{-1}]	Ref
[Fe-Fe]	Fe$^{III}_4$[Fe^{II}(CN)$_6$]$_3$	N/A	2	N/A	[55]
[Co-Fe]	Co$_3$[Fe(CN)$_6$]$_2$	4.5×10^{-4}	52	N/A	[47]
[Co-Co]	Co$_3$[Co(CN)$_6$]$_2$	8.1×10^{-4}	88	N/A	[47]
[Co-CoPt]	[Co^{II}(H$_2$O)$_2$]$_n$[Co^{III}(CN)$_6$]$_{0.63}$[Pt^{II}(CN)$_4$]$_{0.37}$	N/A	50% 450 nm light	N/A	[57]
[Fe$_{0.75}$Co$_{0.25}$-Co]	(Fe$_{0.75}$Co$_{0.25}$)$_3$[Co(CN)$_6$]$_2$	N/A	6.9	N/A	[58]
[Co-Co]	Co$_3$[Co(CN)$_6$]$_2$	N/A	N/A	N/A	[58]
[CaCo-Co]	Ca$_{0.06}$Co$^{II}_{1.44}$Co^{III}(CN)$_6$	N/A	200	N/A	[59]
[CoFe-TPyP]	Co$_6$[(Fe(CN)$_5$)$_4$-porphyrin]	3.2×10^{-4}	N/A	2.2	[60]
[CoFe-Ru]	Na$_{0.96}$Co$_{2.86}$[Fe(CN)$_5$]$_{2.13}$-[P4VP]$_6$-[Ru(bpy)$_2$]Cl$_{2.29}$	4.5×10^{-4}	N/A	1.85	[61]
[CoFe]@[CoCo]	[Cu$^{II}_{1.5}$[Fe^{III}(CN)$_6$]@[Co$^{II}_{1.5}$Co^{III}(CN)$_6$]	N/A	N/A	2.05	[41]
[CuCo]@[CoCo]	[Cu$^{II}_{1.5}$[Co^{III}(CN)$_6$]@[Co$^{II}_{1.5}$Co^{III}(CN)$_6$]	N/A	N/A	1.5	[41]
[CoPt]@[CoCo]	[Co^{II}[Pt^{IV}(CN)$_6$]@[Co$^{II}_{1.5}$Co^{III}(CN)$_6$]	N/A	N/A	1.5	[41]

crease in the quantum yield up to 200% when a small quantity of calcium ions (Ca/Co atomic ratio is 0.042) is incorporated into the polymeric cyanide structure.

The Lewis acidity of calcium ions is assumed to play an important role similar to its effect in the natural photosynthetic process. Although the proper energy levels and a long excited-state lifetime of the Ru(bpy)$_3^{2+}$ complex makes it one of the most widely studied photosensitizers, it suffers from easy photodecomposition, thereby limiting its use for long-term photocatalytic studies and scalable applications. Our group has shown that the stability of a ruthenium pyridyl PS could be enhanced by immobilizing it within a PB structure by utilizing a polymer as a bridging platform.[61] A non-ruthenium analog, porphyrin PS/PB assembly was prepared later, which has a similar TOF (3.2×10^{-4} s^{-1}) and high stability similar to its ruthenium analogs.[60] It exhibits outstanding stability throughout a 3 h photocatalytic test and has the potential to be implemented owing to its facile synthetic pathway. This finding also paves the way for the development of robust and efficient heterogeneous PB-based dye-sensitized photoelectrodes for water oxidation (see Section 2.4 for more detail).

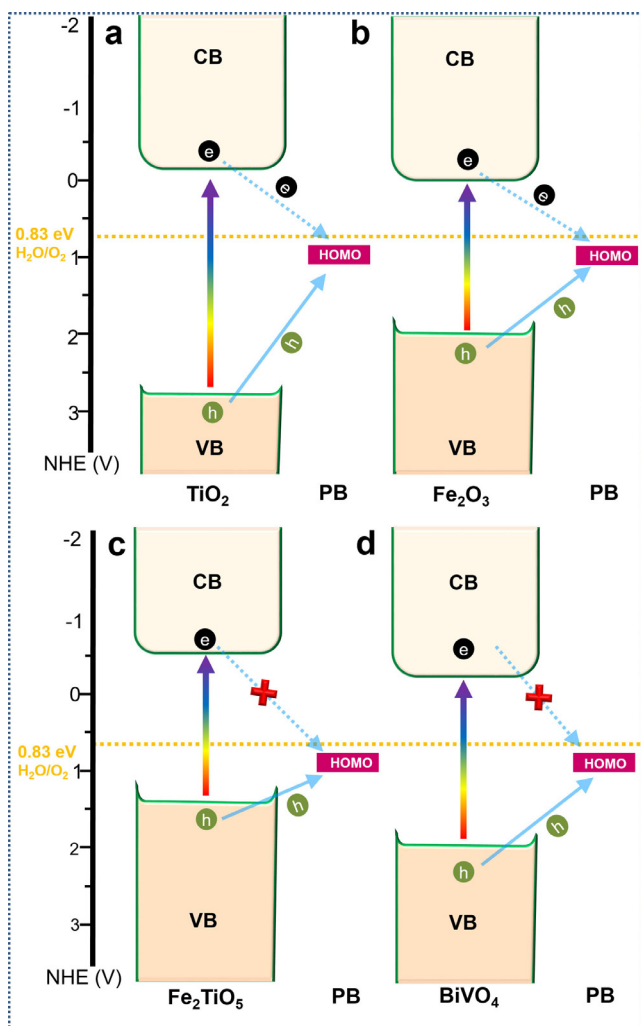## 2.3 Photoelectrochemical (PEC) water oxidation

Photocatalytic studies encouraged scientists to couple PBA-based WOCs with proper SCs for the development of water oxidation photoanodes. One of the main criteria for the prepara-tion of such a photoelectrode is the proper match between the energy levels of different components. The PEC process is initiated with the excitation of the electrons in the SC from the valance band (VB) to the conduction band (CB). Then, once there is a proper energy match, the electrons from the PB catalyst are transferred to the SC VB, which leads to the oxidation of cobalt sites to become active catalysts for water oxidation. The expected PEC mechanism is slightly different from the photocatalytic one, in which the electrons are transferred from PB to the SC rather than the chromophore, and then to the cathodic compartment, which is a standard Pt metallic electrode (Figure 5 a). The proposed mechanism is similar to the photocatalytic process, which is initiated by the utilization of photons by the SC to yield electrons in the CB and holes in the VB (Figure 5 b).

The holes are then transferred to the cobalt sites to activate them for the water oxidation process. For an efficient charge transfer, the VB of the SC should be placed at a slightly lower energy level than the HOMO level of the PB. Furthermore, the relative energy difference between the VB of SC and the HOMO level of PB ($\Delta_{HOMO-VB}$) and that between the CB of SC and the HOMO level of PB ($\Delta_{CB-HOMO}$) could be compared to evaluate their performances. The effect of the energy level alignment on the performance of PBA-coated semiconductors is shown in Figure 6. To date, various SCs have been coupled with PBAs to realize water oxidation photoanodes, as shown in Table 3. All of the SCs studied up to now have lower VB
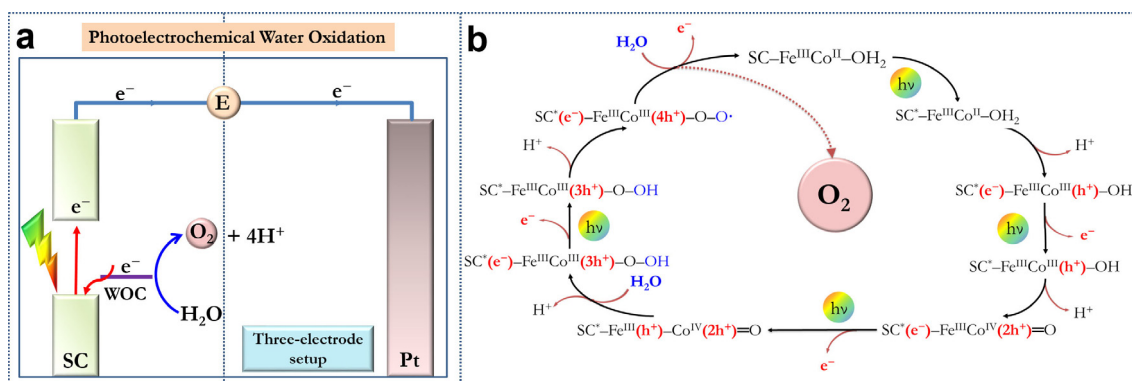
Figure 5. Schematic of (a) a general PEC water oxidation setup, including a photoanode that consists of a SC and WOC immersed in an electrolyte, and (b) the responsible PCET mechanism for PEC water oxidation with CoFe PBAs.

Chemistry–A European Journal

Minireview
doi.org/10.1002/chem.202004091

Chemistry Europe
European Chemical
Societies Publishing

Figure 6. Schematic illustration of band energy levels for different CoFe PBA incorporated SC photoelectrodes under neutral conditions, pH 7: (a) PB/TiO$_2$, (b) PB/Fe$_2$O$_3$, (c) PB/Fe$_2$TiO$_5$, and (d) PB/BiVO$_4$. The ideal band alignment requires a condition in which ($\Delta_{HOMO-VB}$) should be smaller than ($\Delta_{CB-HOMO}$). As both PB/Fe$_2$TiO$_5$ and PB/BiVO$_4$ meet this condition, they have less probability of photoexcited carrier recombination (shown as a red cross) at the HOMO level of PB compared with the other two systems.

energy levels than the HOMO of CoFe PBA. In the case of PB/TiO$_2$, the CB is located at closer proximity compared with the VB, which results in poor PEC performance owing to electron–

hole recombination between the CB of SC and HOMO level of PB.[68] In this case, the PB structure acts as a trapping center that mediates the electron–hole pair recombination. A similar scenario is also observed for PB/Fe$_2$O$_3$.[66] Galán-Mascarós and co-workers coated Fe$_2$O$_3$ nanowires with a thin layer of TiO$_2$ and upon annealing at high temperature a shell layer of Fe$_2$TiO$_5$ was formed. In this way, the energy levels (VB and CB) of Fe$_2$O$_3$ shift upwardly for a better energy level alignment.[67] This modification yields a photocurrent density of 1.25 mA cm^{-2} at 1.23 V$_{RHE}$, which is almost one order of magnitude higher than the pristine Fe$_2$O$_3$ nanowires. BiVO$_4$, on the other hand, inherently has a proper band energy alignment among the recently employed SCs in this field. Both CoCo and CoFe PBAs enhance the photocurrent densities when they are coupled to BiVO$_4$.[63–65] Transient absorption measurements reveal that a PBA coating enhances the performance by presenting a favorable interface for efficient hole transfer, thereby retarding recombination in the semiconductor, combined with the catalytic function necessary to drive water oxidation.[62]

Pires et al. also examined the use of cobalt pentacyanoferrate derivatives with different auxiliary ligands (CoFe-L; L = CN, NH$_3$, isn, and mpz) on PEC performances of BiVO$_4$ photoanodes and investigated the effect of the ligand on the relative alignments of the band edges.[70] They observed that the modification of Fe(CN)$_5$ precursors lead to less unfavorable loss of charge transport mobility and a favorable effect on the photocurrent generation compared with the hexacyanoferrate analog. PBA-coated BiVO$_4$ electrodes have also been coupled with Au plasmonic nanoparticles to further enhance the photocurrent performance under neutral conditions.[69] The resulting plasmonic-catalyst hybrid design exhibits a photocurrent density as high as 1.33 mA cm^{-2} at 1.23 V$_{RHE}$. This study, in particular, shows that the diverse and facile cyanide chemistry allows the incorporation of proper units into cyanide-based photoelectrodes.
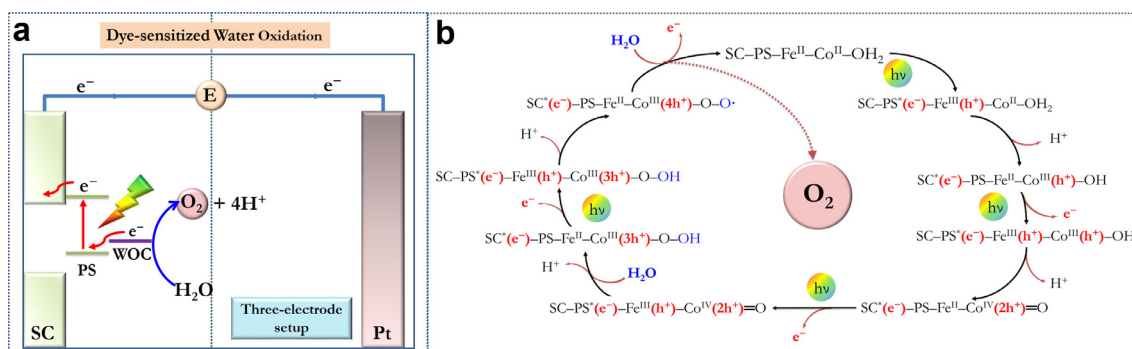
2.4 Dye-Sensitized photoelectrochemistry

In addition to the mechanisms proposed above, PB assemblies have also been utilized to develop dye-sensitized water oxidation photoanodes. In this assembly, the dye acts as a molecular visible light absorbing material to generate electron–hole pairs, as shown in Figure 7a. The proposed mechanism in-

Table 3. A summary of PEC performances of PB-based photoelectrodes.

Photoanode[a]	j @1.23 V$_{RHE}$ [mA cm^{-2}][b]	Illumination	Electrolyte	Ref
[Co-Fe^{III}]/BiVO$_4$	≈1.1	450 W Xe lamp; AM 1.5 solar filter; 1 sun (100 mW cm^{-2})	pH 7 (0.1 M KPi buffer)[c]	[62]
[Co-Fe^{III}]/BiVO$_4$	0.92	450 W Xe lamp; AM 1.5 solar filter; 1 sun (100 mW cm^{-2})	pH 7 (0.1 M KPi buffer)	[63]
[Co-Co^{III}]/BiVO$_4$	≈0.25	AM 1.5 solar filter; (100 mW cm^{-2})	pH 7 (0.2 M K$_2$SO$_4$)	[64]
[Co-Co^{III}]/V$_2$O$_5$/BiVO$_4$	≈0.63	N/A; solar spectrum	N/A: aqueous solution	[65]
[Co-Fe^{III}]/Fe$_2$O$_3$	≈0.23	450 W Xe lamp; AM 1.5 solar filter; 1 sun (100 mW cm^{-2})	pH 7 (0.1 M KPi buffer)	[66]
[Co-Fe^{III}]/Fe$_2$TiO$_5$/Fe$_2$O$_3$	1.25	150 W Xe lamp; AM 1.5 solar filter; 1 sun (100 mW cm^{-2})	pH 1 (0.1 M NaNO$_3$ + 0.1 M HNO$_3$)	[67]
[Co-Fe^{III}]/TiO$_2$	≈0.5	300 W Xe lamp; AM 1.5 solar filter; 1 sun (100 mW cm^{-2})	pH 7 (0.1 M KPi buffer)	[68]
[Co-Fe^{III}]/BiVO$_4$	1.33	300 W Xe lamp; AM 1.5 solar filter; 1 sun (100 mW cm^{-2})	pH 7 (0.1 M KPi buffer)	[69]

[a] Assemblies are deposited on FTO-coated glass. [b] For those, which do not report potentials versus RHE, the potentials are converted as follows; 1.23 V$_{RHE}$ = 0.62 V$_{Ag/AgCl}$ at pH 7. [c] A 0.1 M solution of potassium phosphate (KH$_2$PO$_4$) buffer at pH 7($\pm$0.1).

Chemistry–A European Journal

Minireview
doi.org/10.1002/chem.202004091

Chemistry
Europe
European Chemical
Societies Publishing

Figure 7. Schematic of (a) a general dye-sensitized PEC water oxidation setup, including a photoanode that consists of a SC and WOC immersed in an electrolyte, and (b) the responsible PCET mechanism for PEC water oxidation with CoFe PBAs.

volves the excitation of the PS with visible light to yield charge separation (Figure 7b). In an ideal scheme, the electrons in the excited state are then transferred to the CB of the SC, which is positioned at a lower energy level compared with the LUMO level of the PS. The holes, which are required for the water oxidation process, are transferred first to iron sites and to catalytic cobalt sites owing to their proper HOMO levels. Therefore, the mechanism implies that iron sites that connect the PS to the cobalt sites could participate also in the charge transfer process.

Molecular and bulk synthetic approaches, both of which have critical drawbacks, have been adopted to develop dye-sensitized photoanodes. Our team has recently proposed a cyanide-based synthetic pathway to take advantage of the strengths of both the molecular approach and the bulk one.[60] In this pathway, the molecular units are connected in a step-by-step fashion similar to the molecular approach, which forms a bulk assembly in the final step. The method enables easy control of the structure of the final product similar to the molecular-based approach. The synthetic protocol is much simpler than that of molecular ruthenium ones as the bridging group between the PS and WOC is a simple cyanide group, which can bind to water oxidation catalytic cobalt sites easily in a one-step reaction. The final bulk assembly exhibits superior stability and a rigid framework under PEC conditions.

The PS and WOC units are connected through a $Fe(CN)_5$ unit, which can easily coordinate to pyridyl-containing organic molecules and polymers.[71–74] This strategy was first used to build an amorphous polymer-bound PB electrocatalyst (Section 2.1).[48] It is then utilized to develop a PS–WOC assembly, which consists of a ruthenium chromophore incorporated into a CoFe PB structure (Section 2.2).[61] We also employed this method to incorporate a pyridyl-containing porphyrin derivative into a CoFe PB structure depicted in Figure 8.[60] Transient absorption and computational studies indicate that the iron site serves as an electron shuttle between the PS and WOC units.

The realization of this versatile pathway prompted us to prepare PB-based dye-sensitized photoanodes. As a proof of concept, a phenazine-based chromophore, Janus Green B (JG), was implemented to a PB structure and then coupled to TiO$_2$ nanowires to develop the first entirely earth-abundant dye-
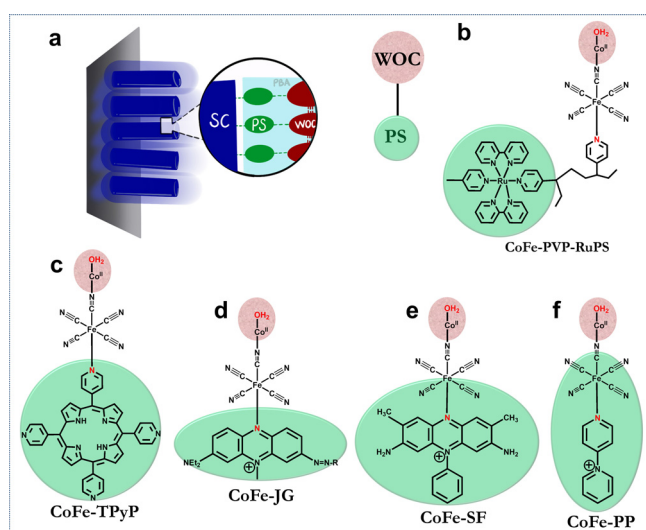

Figure 8. (a) The illustration of a Prussian blue (PB)-based dye-sensitized water oxidation photoanode, in which a PB layer incorporating a PS-WOC assembly is coated over a semiconductor (SC). PB-based PS-WOC assemblies: (b) PVP: poly(4-vinylpyridine), Ru-PS: ruthenium photosensitizer; (c) TPyP: tetrapyridylporphyrin; (d) JG: Janus green B; (e) SF: Safranine O; (f) PP: 4-(pyridyl)pyridinium cation.

sensitized photoanode (CoFe-JG/TiO$_2$).[68] In contrast to bare JG, which decomposes easily under photocatalytic conditions, JG in CoFe-JG/TiO$_2$ retains its structural integrity. Moreover, a photocurrent density of around 60 μA cm^{-2} was achieved at 1.23 V$_{RHE}$ for 2 h under white light coupled to a 420 nm filter.

Another example of a phenazine incorporating derivative as the organic PS is a CoFe PB with Safranin (SF) assembly coated over a visible light absorbing semiconductor, WO$_3$.[75] CoFe-SF/WO$_3$ exhibits a record photocurrent density of 1.3 mA cm^{-2} at just 1.23 V$_{RHE}$, which demonstrates that the easy modification of components in PB-based dye-sensitized photoanodes paves the way for the development of scalable and high-performance water splitting cells.

An interesting feature that we observed in this line of research is the function of the metal site, particularly the iron site in the cyanometalate group. As shown in Figure 9, the cyanometalate group site was used merely as a bridging group (linker) in the majority of the studies. Despite the easily acces-
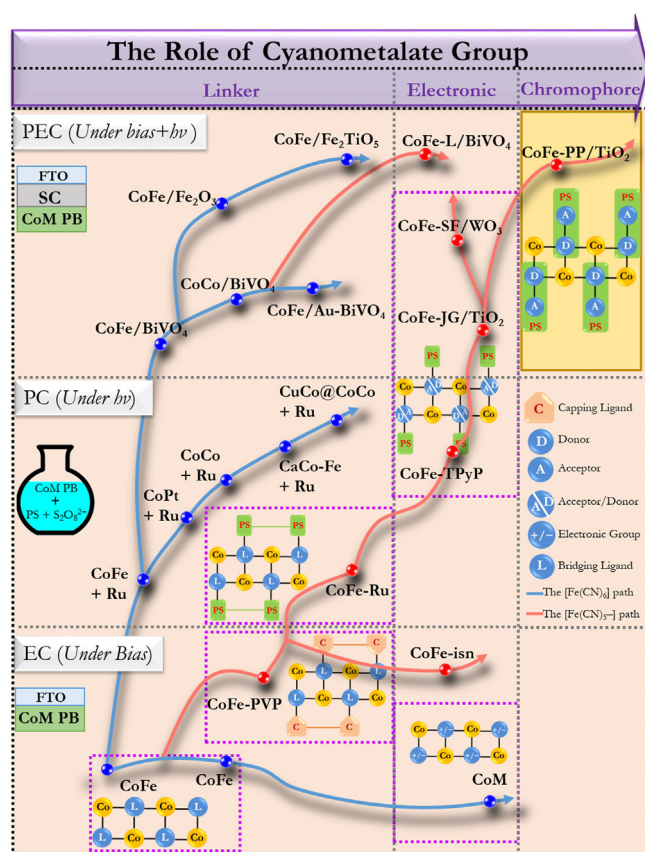
Figure 9. Road map for PB-based water oxidation systems that shows the role of the cyanometalate group in various water oxidation processes including EC, PC, and PEC. Studies highlighted here are as follows: CoFe,[19,35] CoM,[49] CoFe+Ru,[47] CoPt+Ru,[57] CoCo+Ru,[58] CaCo-Fe+Ru,[59] CuCo@Co-Co+Ru,[41] CoFe/BiVO₄,[63] CoCo/BiVO₄,[64] CoFe/AuNPs/BiVO₄,[69] CoFe-L/BiVO₄,[70] CoFe/Fe₂O₃,[66] CoFe/Fe₂TiO₅,[67] CoFe-PVP,[48] CoFe-isn,[51] CoFe-Ru,[61] CoFe-TPyP,[60] CoFe-JG/TiO₂,[68] CoFe-SF/WO₃,[75] CoFe-PP/TiO₂.[88]

sible $Fe^{2+/3+}$ redox process in PBAs, the electronic effect of the iron site was overlooked and the main attention was directed on the cobalt site. Nevertheless, both electrocatalytic and photocatalytic studies, which indicate that CoCo PBAs exhibit relatively higher activities than CoFe PBAs, clearly point out the electronic effect of the cyanometalate group on the catalytic activity of the cobalt sites.

The effect of the iron site is also evident when a chromophore is directly coordinated to CoFe PBA structures. An organic PS could be implemented into the PB structure by using an unconjugated bridging platform as in the case of CoFe-PVP-RuPS.[61] When it is connected directly to the iron site, as in the CoFe-TPyP system, the ground states of the pentacyanoiron(II) and porphyrin groups, which are close in energy, are mixed to form a HOMO comprising Fe d and porphyrin p orbitals.[60] We observed similar behavior when a phenazine-based chromophore, JG, is connected to the iron site to build a CoFe-JG/TiO₂ photoanode for water oxidation.[68] The simplicity and diversity of this methodology allow for the easy modification of components to enhance PEC performance. The electron transfer utilized in these systems constitutes a combination of ligand-to-ligand charge transfer (LLCT), the common feature

observed in organic chromophores, and a metal-to-ligand charge transfer (MLCT), which is a characteristic feature for a metal PS.

In a recent study, we utilized a transparent organic ligand to rule out the LLCT in the charge transfer process. When a pale-yellow solution of $[Fe(CN)_5(NH_3)]^{3-}$ is mixed with a colorless 4-(pyridyl)pyridinium solution (PP⁺), the solution turns into an intense dark-red color thereby indicating the formation of a push–pull iron chromophore, Fe-PP. The donating ability of the Fe^{II} ion surrounded with a five-electron-donating cyanide group and the electron ability of a cationic organic ligand form a donor–acceptor type iron chromophore.[76–82] The cyanide ligand plays an important role in this assembly as the strong-field cyanide ligand increases the octahedral splitting and pushes the undesired metal-centered (MC) orbitals to higher energy levels to avoid possible deactivation pathways, which can compete with the MLCT transition.[83–87] Upon coordination of the iron complex to cobalt ions, the deactivation of MC pathways enhances the excited state lifetime of the iron chromophore above an order of magnitude compared with the uncoordinated complex.[88] Furthermore, the short cyanide group mediates the electron transfer from the cobalt site to the iron site and then to the organic ligand. TiO₂/CoFe-PP, which marks the first example of an iron chromophore utilized water oxidation photoanode, reveals that the iron site can also be promoted to a chromophore.

3. Summary and Outlook

In this review, we identify the key structural parameters in CoFe PBAs, including the role of each component to the catalytic performance to expand our understanding of PB-based water oxidation catalytic assemblies. As the linear coordination of a cyanide ligand to metals allows for the prediction of the structure of the final product and the establishment of a structure and activity correlation, PBAs provide an ideal platform for both fundamental and performance applications.

These materials have been comprehensively studied owing to their superior chemical and physical properties, such as being entirely earth-abundant, having exceptional stability in a wide pH range (1–13), and simple synthetic routes compared with other common WOCs. Various high-performance materials could be derived from nanostructured PB and PBAs. To utilize them for photocurrent generation, they have been coupled with light-absorbing components including photosensitizers and semiconductors, such as TiO₂, Fe₂O₃, Fe₂TiO₅, BiVO₄, and WO₃. These studies point out that each component in the PB structure plays an important role in the catalytic activity. For example, tuning the counter cation enhances the quantum efficiency up to 200% under photocatalytic conditions. The cyanometalate group can be altered not only to enhance the surface concentration but also to increase the TOF of catalytic cobalt sites (synergistic effect). The concentration of cobalt can be diluted by the partial substitution of cobalt sites with relatively low-cost metal ions such as iron and copper. These strategies could be combined to develop efficient PB-based photoanodes.

It should be noted that the catalytic activity of PBAs is highly dependent on the synthetic approach, chemical composition, and crystallinity. Electrical conductivity decreases as the thickness of the PBA layer increases thereby resulting in high overpotentials and low catalytic efficiency. The optimum synthetic conditions for the ideal thickness and morphology of PBAs should, therefore, be explored systematically by using the strategies discussed throughout this review.

Co-based PBAs have been the main focus as other metal ions exhibit poor activities under either electrocatalytic and/or photocatalytic activities. The investigation of non-cobalt PBA coupled with proper SCs could be an interesting venue to elucidate the effect of band energy alignment in semiconductor/catalyst photoelectrodes. On the other hand, decreasing the cyanide number either in the iron PS case or the integration of PB into an organic chromophore case can be advantageous when they are combined with semiconductors that are observed to exhibit poor performance with regular CoFe PBAs. In this respect, the utilization of CoFe PBAs can be extended in several different promising directions. It is then clear that a lot is still waiting to be discovered. Further research in these areas will accelerate the development of new, stable chromophores, catalysts, and their combinations (dyads, triads, etc.). Opportunities can come with challenges, but recent advances in the field indicate that PBAs hold the potential to play a significant role in developing scalable and efficient water splitting cells.

Acknowledgments

Conflict of interest

The authors declare no conflict of interest.

[1] K. R. Dunbar, R. A. Heintz, *Chemistry of Transition Metal Cyanide Compounds: Modern Perspectives*, Wiley, New York, **1997**.
[2] Z. Qin, Y. Li, N. Gu, *Adv. Healthcare Mater.* **2018**, *7*, 1800347.
[3] S. Kitagawa, R. Kitaura, S. Noro, *Angew. Chem. Int. Ed.* **2004**, *43*, 2334 – 2375; *Angew. Chem.* **2004**, *116*, 2388 – 2430.
[4] Y. S. Meng, O. Sato, T. Liu, *Angew. Chem. Int. Ed.* **2018**, *57*, 12216 – 12226; *Angew. Chem.* **2018**, *130*, 12394 – 12405.
[5] M. J. P. Muñoz, E. C. Martínez, *Prussian Blue Based Batteries*, Springer, Cham, **2018**.
[6] J. A. Hill, A. L. Thompson, A. L. Goodwin, *J. Am. Chem. Soc.* **2016**, *138*, 5886 – 5896.
[7] J. M. Herrera, A. Bachschmidt, F. Villain, A. Bleuzen, V. Marvaud, W. Wernsdorfer, M. Verdaguer, *Phil. Trans. R. Soc. A* **2008**, *366*, 127 – 138.
[8] D. Aguilà, Y. Prado, E. S. Koumousi, C. Mathonière, R. Clérac, *Chem. Soc. Rev.* **2016**, *45*, 203 – 224.
[9] Y. Lu, L. Wang, J. Cheng, J. B. Goodenough, *Chem. Commun.* **2012**, *48*, 6544 – 6546.
[10] B. Wang, Y. Han, X. Wang, N. Bahlawane, H. Pan, M. Yan, Y. Jiang, *iScience* **2018**, *3*, 110 – 133.
[11] C. Deng, D. Wang, *Batter. Supercaps.* **2019**, *2*, 290 – 310.
[12] S. S. Kaye, J. R. Long, *J. Am. Chem. Soc.* **2005**, *127*, 6506 – 6507.
[13] F. Karadas, H. El-Faki, E. Deniz, C. T. Yavuz, S. Aparicio, M. Atilhan, *Microporous Mesoporous Mater.* **2012**, *162*, 91 – 97.
[14] A. A. Karyakin, *Electroanalysis* **2001**, *13*, 813 – 819.
[15] A. A. Karyakin, E. E. Karyakina, L. Gorton, *Electrochem. Commun.* **1999**, *1*, 78 – 82.
[16] L. M. N. Assis, R. Leones, J. Kanicki, A. Pawlicka, M. M. Silva, *J. Electroanal. Chem.* **2016**, *777*, 33 – 39.
[17] L. Hedley, L. Porteous, D. Hutson, N. Robertson, J. O. Johansson, *J. Mater. Chem. C* **2018**, *6*, 512 – 517.
[18] M. Shokouhimehr, E. S. Soehnlen, J. Hao, M. Griswold, C. Flask, X. Fan, J. P. Basilion, S. Basu, S. D. Huang, *J. Mater. Chem.* **2010**, *20*, 5251 – 5259.
[19] S. Pintado, S. Goberna-Ferrón, E. C. Escudero-Adán, J. R. Galán-Mascarós, J. R. G.-M. Sara Pintado, S. Goberna-Ferrón, E. C. Escudero-Adán, *J. Am. Chem. Soc.* **2013**, *135*, 13270 – 13273.
[20] T. G. U. Ghobadi, A. Ghobadi, E. Ozbay, F. Karadas, *ChemPhotoChem* **2018**, *2*, 161 – 182.
[21] A. Ghobadi, T. G. Ulusoy Ghobadi, F. Karadas, E. Ozbay, *Adv. Opt. Mater.* **2019**, *7*, 1900028.
[22] B. Singh, A. Indra, *Mater. Today Energy* **2020**, *16*, 100404.
[23] L. M. Cao, D. Lu, D. C. Zhong, T. B. Lu, *Coord. Chem. Rev.* **2020**, *407*, 213156.
[24] C. Xuan, J. Zhang, J. Wang, D. Wang, *Chem. Asian J.* **2020**, *15*, 958 – 972.
[25] J. Chen, L. Wei, A. Mahmood, Z. Pei, Z. Zhou, X. Chen, Y. Chen, *Energy Storage Mater.* **2020**, *25*, 585 – 612.
[26] D. M. Dongni Zhao, Y. Lu, *Molecules* **2020**, *25*, 2304.
[27] D. A. Lutterman, Y. Surendranath, D. G. Nocera, *J. Am. Chem. Soc.* **2009**, *131*, 3838 – 3839.
[28] M. W. Kanan, D. G. Nocera, *Science* **2008**, *321*, 1072 – 1075.
[29] X. Liang, Z. Deng, L. Jing, X. Li, Z. Dai, C. Li, M. Huang, *Chem. Commun.* **2013**, *49*, 11029 – 11032.
[30] G. Liang, J. Xu, X. Wang, *J. Am. Chem. Soc.* **2009**, *131*, 5378 – 5379.
[31] Y. Liu, X. Wang, *Polym. Chem.* **2012**, *3*, 2632 – 2639.
[32] S. S. Kaye, J. R. Long, *Chem. Commun.* **2007**, 4486 – 4488.
[33] T. Li, F. He, Y. D. Dai, *J. Radioanal. Nucl. Chem.* **2016**, *310*, 1139 – 1145.
[34] F. H. Köhler, O. Storcheva, *Inorg. Chem.* **2015**, *54*, 6801 – 6806.
[35] L. Han, P. Tang, A. Reyes-Carmona, B. Rodriguez-Garcia, M. Torrens, J. R. Morante, J. Arbiol, J. R. Galán-Mascarós, *J. Am. Chem. Soc.* **2016**, *138*, 16037 – 16045.
[36] P. J. Faustino, Y. Yang, J. J. Progar, C. R. Brownell, N. Sadrieh, J. C. May, E. Leutzinger, D. A. Place, E. P. Duffy, F. Houn, S. A. Loewke, V. J. Mecozzi, C. D. Ellison, M. A. Khan, A. S. Hussain, R. C. Lyon, *J. Pharm. Biomed. Anal.* **2008**, *47*, 114 – 125.
[37] D. F. Thompson, C. O. Church, *Pharmacotherapy* **2001**, *21*, 1364 – 1367.
[38] M. A. Miller, M. M. Patel, T. Coon, *Hosp. Pharm.* **2005**, *40*, 796 – 797.
[39] A. Mohammad, Y. Yang, M. A. Khan, P. J. Faustino, *Clin. Toxicol.* **2015**, *53*, 102 – 107.
[40] R. O. Lezna, R. Romagnoli, N. R. De Tacconi, K. Rajeshwar, N. R. De Tacconi, K. Rajeshwar, *J. Phys. Chem. B* **2002**, *106*, 3612 – 3621.
[41] H. Tabe, A. Kitase, Y. Yamada, *Appl. Catal. B Environ.* **2020**, *262*, 118101.
[42] C. Díaz, A. Arancibia, *Inorganica Chim. Acta* **1998**, *269*, 246 – 252.
[43] L. T. Zhang, X. Q. Zhu, S. M. Hu, Y. X. Zhang, S. D. Su, Y. Y. Yang, X. T. Wu, T. L. Sheng, *Dalton Trans.* **2019**, *48*, 7809 – 7816.
[44] W. M. Laidlaw, A. L. Thompson, R. G. Denning, *Dalton Trans.* **2013**, *42*, 4695 – 4703.
[45] E. J. Schelter, F. Karadas, C. Avendano, A. V. Prosvirin, W. Wernsdorfer, K. R. Dunbar, *J. Am. Chem. Soc.* **2007**, *129*, 8139 – 8149.
[46] F. Karadas, E. J. Schelter, M. Shatruk, A. V. Prosvirin, J. Bacsa, D. Smirnov, A. Ozarowski, J. Krzystek, J. Telser, K. R. Dunbar, *Inorg. Chem.* **2008**, *47*, 2074 – 2082.
[47] S. Goberna-Ferrón, W. Y. Hernández, B. Rodríguez-García, J. R. Galán-Mascarós, *ACS Catal.* **2014**, *4*, 1637 – 1641.
[48] M. Aksoy, S. V. K. Nune, F. Karadas, *Inorg. Chem.* **2016**, *55*, 4301 – 4307.
[49] E. P. Alsaç, E. Ülker, S. V. K. Nune, Y. Dede, F. Karadas, *Chem. Eur. J.* **2018**, *24*, 4856 – 4863.
[50] A. Eftekhari, *Mater. Today Energy* **2017**, *5*, 37 – 57.

[51] B. M. Pires, P. L. Dos Santos, V. Katic, S. Strohauer, R. Landers, A. L. B. For-miga, J. A. Bonacin, *Dalton Trans.* **2019**, *48*, 4811 – 4822.

[52] B. Rodríguez-García, Á. Reyes-Carmona, I. Jiménez-Morales, M. Blasco-Ahicart, S. Cavaliere, M. Dupont, D. Jones, J. Rozière, J. R. Galán-Mascarós, F. Jaouen, *Sustainable Energy Fuels* **2018**, *2*, 589 – 597.

[53] F. Karadas, *Turkish J. Chem.* **2019**, *43*, 511 – 519.

[54] L. Han, J. R. Galán-Mascarós, *Catalysts* **2020**, *10*, 130.

[55] M. Kaneko, A. Yamada, *Electrochim. Acta* **1986**, *31*, 273 – 275.

[56] P. A. Christensen, A. Harriman, *J. Chem. Soc. Faraday Trans.* **1985**, *81*, 2461 – 2466.

[57] Y. Yamada, K. Oyama, R. Gates, S. Fukuzumi, *Angew. Chem. Int. Ed.* **2015**, *54*, 5613 – 5617; *Angew. Chem.* **2015**, *127*, 5705 – 5709.

[58] Y. Isaka, K. Oyama, Y. Yamada, T. Suenobu, S. Fukuzumi, *Catal. Sci. Technol.* **2016**, *6*, 681 – 684.

[59] Y. Yamada, K. Oyama, T. Suenobu, S. Fukuzumi, *Chem. Commun.* **2017**, *53*, 3418 – 3421.

[60] T. G. Ulusoy Ghobadi, E. Akhuseyin Yildiz, M. Buyuktemiz, S. Sadigh Ak-bari, D. Topkaya, Ü. İsci, Y. Dede, H. G. Yaglioglu, F. Karadas, *Angew. Chem. Int. Ed.* **2018**, *57*, 17173 – 17177; *Angew. Chem.* **2018**, *130*, 17419 – 17423.

[61] Z. Kap, F. Karadas, *Faraday Discuss.* **2019**, *215*, 111 – 122.

[62] B. Moss, F. S. Hegner, S. Corby, S. Selim, L. Francàs, N. López, S. Giménez, J. R. Galán-Mascarós, J. R. Durrant, *ACS Energy Lett.* **2019**, *4*, 337 – 342.

[63] F. S. Hegner, I. Herraiz-Cardona, D. Cardenas-Morcoso, N. López, J. R. Galán-Mascarós, S. Gimenez, *ACS Appl. Mater. Interfaces* **2017**, *9*, 37671 – 37681.

[64] K. Trzciński, M. Szkoda, K. Szulc, M. Sawczak, A. Lisowska-Oleksiak, *Electrochim. Acta* **2019**, *295*, 410 – 417.

[65] K. Trzciński, M. Szkoda, M. Sawczak, A. Lisowska-Oleksiak, *Electrocatalysis* **2020**, *11*, 180 – 187.

[66] F. S. Hegner, D. Cardenas-Morcoso, S. Giménez, N. López, J. R. Galán-Mascarós, *ChemSusChem* **2017**, *10*, 4552 – 4560.

[67] P.-Y. Tang, L.-J. Han, F. S. Hegner, P. Paciok, B.-P. Martia, H.-C. Du, X.-K. Wei, L. Jin, H.-B. Xie, Q. Shi, T. Andreu, L.-C. Monica, M. Heggen, R. E. Dunin-Borkowski, N. Lopez, J. R. Galán-Mascarós, J. R. Morante, J. Arbiol, *Adv. Energy Mater.* **2019**, 1901836.

[68] T. G. Ulusoy Ghobadi, A. Ghobadi, M. Buyuktemiz, E. Akhuseyin Yildiz, D. B. Yildiz, H. G. Yaglioglu, Y. Dede, E. Ozbay, F. Karadas, *Angew. Chem. Int. Ed.* **2020**, *59*, 4082 – 4090; *Angew. Chem.* **2020**, *132*, 4111 – 4119.

[69] T. G. Ulusoy Ghobadi, A. Ghobadi, M. C. Soydan, M. Barzgar Vishlaghi, S. Kaya, F. Karadas, E. Ozbay, *ChemSusChem* **2020**, *13*, 2577 – 2588.

[70] B. M. Pires, F. S. Hegner, J. A. Bonacin, J. R. Galan-Mascaros, *ACS Appl. Energy Mater.* **2020**, *3*, 8448 – 8456.

[71] D. H. Macartney, *Rev. Inorg. Chem.* **1988**, *10*, 101 – 152.

[72] H. Huang, W. Chen, C. Yang, A. Yeh, *Inorg. Chem.* **1991**, *11*, 1862 – 1868.

[73] S. A. V. Jannuzzi, B. Martins, M. I. Felisberti, A. L. B. Formiga, *J. Phys. Chem. B* **2012**, *116*, 14933 – 14942.

[74] A. J. Baer, D. H. Macartney, *Inorg. Chem.* **2000**, *39*, 1410 – 1417..

[75] T. G. Ulusoy Ghobadi, A. Ghobadi, M. Demirtas, R. Phul, E. A. Yildiz, H. G. Yaglioglu, E. Durgun, E. Ozbay, F. Karadas, *Cell. Rep. Phys. Sci.* https://doi.org/10.1016/j.xcrp.2020.100319.

[76] I. Deligkiozi, E. Voyiatzis, A. Tsolomitis, R. Papadakis, *Dye Pigment.* **2015**, *113*, 709 – 722.

[77] L. M. Baraldo, P. Forlano, A. R. Parise, L. D. Slep, J. A. Olabe, *Coord. Chem. Rev.* **2001**, *219 – 221*, 881 – 921.

[78] B. J. Coe, J. L. Harries, M. Helliwell, L. A. Jones, I. Asselberghs, K. Clays, B. S. Brunschwig, J. A. Harris, J. Garin, J. Orduna, *J. Am. Chem. Soc.* **2006**, *128*, 12192 – 12204.

[79] B. J. Coe, S. P. Foxon, E. C. Harper, J. Raftery, R. Shaw, C. A. Swanson, I. Asselberghs, K. Clays, B. S. Brunschwig, A. G. Fitch, *Inorg. Chem.* **2009**, *48*, 1370 – 1379.

[80] H. E. Toma, C. Creutz, *Inorg. Chem.* **1977**, *16*, 545 – 550.

[81] R. Papadakis, A. Tsolomitis, *J. Phys. Org. Chem.* **2009**, *22*, 515 – 521.

[82] R. Papadakis, *J. Phys. Chem. B* **2016**, *120*, 9422 – 9433.

[83] M. Yang, D. W. Thompson, G. J. Meyer, *Inorg. Chem.* **2000**, *39*, 3738 – 3739.

[84] M. Yang, D. W. Thompson, G. J. Meyer, *Inorg. Chem.* **2002**, *41*, 1254 – 1262.

[85] S. Ardo, G. J. Meyer, *Chem. Soc. Rev.* **2009**, *38*, 115 – 164.

[86] E. Jakubikova, D. N. Bowman, *Acc. Chem. Res.* **2015**, *48*, 1441 – 1449.

[87] D. N. Bowman, J. H. Blew, T. Tsuchiya, E. Jakubikova, *Inorg. Chem.* **2013**, *52*, 8621 – 8628.

[88] T. Gamze, U. Ghobadi, A. Ghobadi, M. Demirtas, M. Buyuktemiz, K. N. Ozvural, E. A. Yıldız, E. Erdem, H. G. Yaglioglu, E. Durgun, Y. Dede, E. Ozbay, F. Karadas, unpublished results.